Optical absorption of $KZnF_3:Tl^+$ and $KMgF_3:Tl^+$ crystals

2001 J. Phys.: Condens. Matter 13 6247

(http://iopscience.iop.org/0953-8984/13/28/307)

INSTITUTE OF PHYSICS PUBLISHING JOURNAL OF PHYSICS: CONDENSED MATTER

J. Phys.: Condens. Matter **13** (2001) 6247–6258 PII: S0953-8984(01)21699-3

Optical absorption of $KZnF_3$:Tl^+ and $KMgF_3$:Tl^+ crystals

L K Aminov, A V Kosach, S I Nikitin, N I Silkin[1] and R V Yusupov

Kazan State University, Kremlevskaya 18, 420008 Kazan, Russia

E-mail: nikolai.silkin@ksu.ru

Received 7 February 2001, in final form 25 April 2001
Published 29 June 2001
Online at stacks.iop.org/JPhysCM/13/6247

Abstract

The absorption spectra of $KZnF_3$:Tl^+ and $KMgF_3$:Tl^+ crystals have been measured over the energy range 1.5–6.4 eV at temperatures of 10–300 K. A wide absorption band with a clear doublet structure identified as an absorption A band of Tl^+ impurity centres is observed for both crystals. The position of the band, its bandwidth and the distribution of absorption intensity between the two components of the band are temperature dependent in the range $T > 65$ K.

All features of the absorption spectra of the crystals studied are explained within the frameworks of the conventional theory on the basis of the Frank–Condon principle and the semiclassical picture of crystal lattice vibrations. The band shapes calculated by the Monte Carlo method are in satisfactory agreement with observed ones.

1. Introduction

Crystals of alkali halides doped with mercury-like ions have been traditional objects of experimental and theoretical investigation for several decades; a number of reviews are devoted to optical properties of such crystals [1–3]. Fluorine crystals doped with ions having an external ns^2 shell ('s^2 ions') are much less investigated, though these objects are interesting as active materials for tunable solid-state lasers and scintillators [4–6]. Among the fluorine compounds the perovskite-like ABF_3 crystals are of special interest. Due to the high symmetry and technological efficiency of the growth process these crystals are good model objects for fundamental studies and in some cases they are of great practical value. Thus, $KZnF_3$ crystals activated by Cr^{3+}, Co^{2+} and Ni^{2+} ions and $KMgF_3$ crystals with colour centres are used as active media for lasers in the near-infrared region [7–9].

We have investigated the optical properties of $KZnF_3$:Tl^+ and $KMgF_3$:Tl^+ crystals, and in this work we report the results of the absorption spectra analysis. The absorption and luminescence spectra of Tl^+ centres in $KZnF_3$ crystal are slightly shifted to the long-wavelength region in comparison with those for $KMgF_3$ crystal, studied previously by Scacco *et al* [10,11].

[1] Author to whom any correspondence should be addressed. Telephone: (007 8432) 315585.

The general picture of the absorption spectrum, the structure and the widths of the absorption bands in the fluoroperovskites $KMgF_3$ and $KZnF_3$ doped with Tl^+ ions are similar to those for alkali halide crystals. In both types of crystal, thallium centres are believed to possess cubic symmetry: the admixed ion and its nearest surroundings form an octahedral complex $[TlF_6]^{5-}$ in alkali halides, while in fluoroperovskites they form a complex, $[TlF_{12}]^{11-}$, with fluorine ions at the centres of the cube edges (figure 1), the Zn^{2+} (Mg^{2+}) ions being at cube apices.

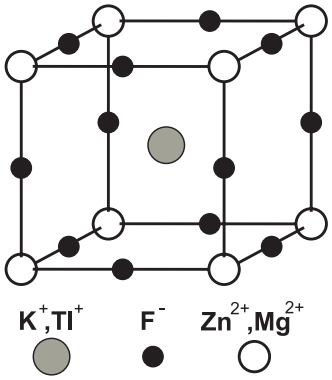

Figure 1. The unit cell for the $KZnF_3$:Tl^+ and $KMgF_3$:Tl^+ crystals.

A cubic crystal field does not split the electronic p states of Tl^+ ions; therefore the energy level schemes spanning the states of the ground $6s^2$ and the first excited 6s6p configurations (figure 2) look qualitatively the same for a free ion and for an ion at any lattice site with cubic symmetry. The scheme is not changed if the atomic single-electron s and p functions are replaced by the corresponding molecular orbitals of a_{1g} and t_{1u} types.

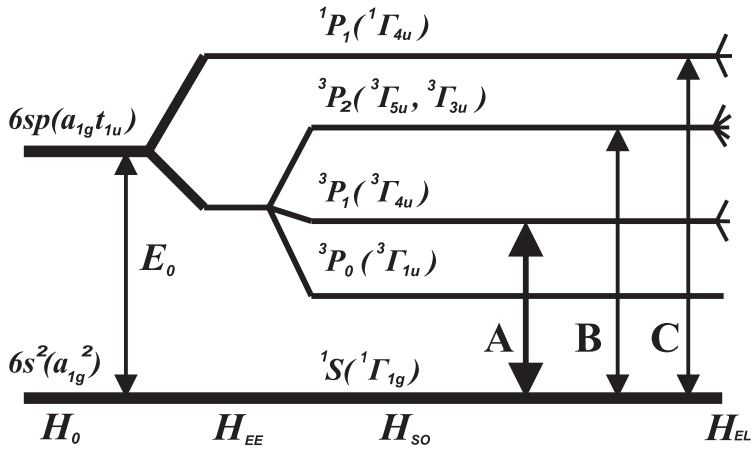

Figure 2. Energy levels of an s^2 ion in a crystal field of cubic symmetry.

The broadening of the absorption lines (formation of bands) in crystals and the band structure are due to the crystal lattice vibrations. The appropriate theory, on the basis of the Jahn–Teller effect, the semiclassic picture of vibrations and the Frank–Condon principle, was elaborated in detail and widely used for interpretation of different optical phenomena in doped alkali halide crystals (see [1–3]). We will use this theory in a slightly modified form to analyse our measurements, considering three vibrational modes.

In the next section the experimental part of the study is presented. Then we reproduce the principal points of the conventional theory with some modifications which allow us to consider in a unified form the linear electron–lattice interactions and those that are quadratic in atomic displacements, and to take into account the differences of the effective frequencies of the interaction modes. Also some misprints which are present in several frequently cited papers are corrected. Further, we present the results of modelling the absorption spectra with the Monte Carlo method and compare our results with the previous data for $KMgF_3$ crystal [10, 12]. The luminescence spectra of $KZnF_3$:Tl^+ and $KMgF_3$:Tl^+ crystals will be discussed in a forthcoming paper.

2. Experimental procedure and results

The $KZnF_3$ and $KMgF_3$ single crystals were grown from the melt in graphite crucibles by the Bridgman–Stockbarger method. Dried KF and ZnF_2 or MgF_2, purified by recrystallization from the melt, were used as starting materials. Thallium fluoride, TlF, was used to activate the crystals by means of Tl^+ ions. The concentration of TlF in the melt was 0.5 mol%. The crystals were grown in an argon atmosphere fluorinated by the gaseous products of Teflon pyrolysis. The samples grown were of good optical quality and had a cylindrical form 10 mm in diameter and up to 50 mm in length.

The absorption spectra were measured over the energy range 1.5–6.4 eV using a Specord-M40 spectrophotometer. To investigate the temperature dependencies in the range 10–300 K, an Oxford Instruments CF-1204 optical cryostat was used.

In the frequency range studied, one wide absorption band is observed for both $KZnF_3$:Tl^+ and $KMgF_3$:Tl^+ crystals, which has a clear doublet structure at room temperature with the maxima positions at 5.93 and 6.05 eV for $KZnF_3$:Tl^+, and 6.04 and 6.18 eV for $KMgF_3$:Tl^+. The band shape is practically unchanged in the temperature range 10–65 K. The shapes of the absorption bands at 10, 150 and 300 K are shown in figure 3 ($KZnF_3$:Tl^+) and figure 4 ($KMgF_3$:Tl^+). The absorption data for $KMgF_3$:Tl^+ almost completely correspond to the absorption A-band data for the same crystal obtained previously in [10].

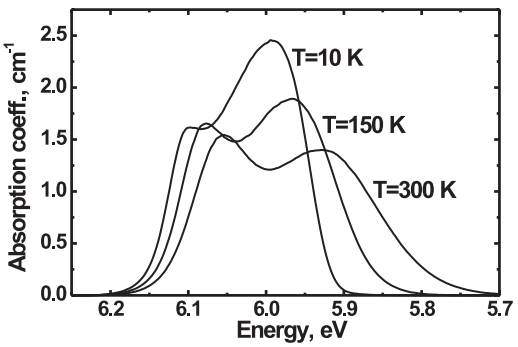

Figure 3. The temperature dependence of the absorption A band of the Tl^+ ion in the $KZnF_3$ crystal.

As the temperature decreases, the bandwidth decreases, maxima shift to higher energies and the intensity redistributes to the benefit of a long-wavelength component, the integral intensity being constant. The absence of temperature dependence of the band integral intensity evidences that this band corresponds to an allowed transition. Comparison with literature data allows us to attribute the absorption band to the ${}^1\Gamma_{1g} \rightarrow {}^3\Gamma_{4u}$ transition of the Tl^+ centre (A band), the band structure being due to the Jahn–Teller effect in an excited state [1–3, 10].

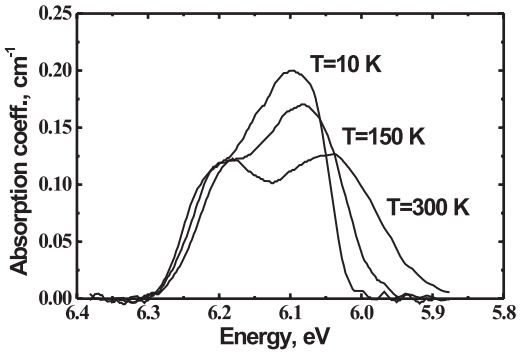

Figure 4. The temperature dependence of the absorption A band of the Tl^+ ion in the $KMgF_3$ crystal.

3. Theoretical model

The initial Hamiltonian for two external electrons of a cubic Tl^+ centre in a crystal is chosen in the adiabatic approximation as follows:

$$H = H_0 + H_{ee} + H_{so} + H_{el} \tag{1}$$

where H_0 is the conventional single-electron approximation for a cubic quasimolecule which may include one or more nearest coordination spheres of the Tl^+ ion, all ions being located at their equilibrium lattice positions. H_{ee} is the Coulomb repulsion between two electrons, H_{so} is the spin–orbit interaction, H_{el} is the electron–lattice interaction which is usually written as an expansion up to the first and second powers of ion displacements from the equilibrium positions:

$$H_{el} = H_{el}^{(1)} + H_{el}^{(2)} = \sum_{\alpha t i} V_i^{(\alpha)}(t) Q_i^{(\alpha)}(t) + \frac{1}{2} \sum_{\alpha t i, \beta t' j} V_{ij}^{(\alpha\beta)}(t, t') Q_i^{(\alpha)}(t) Q_j^{(\beta)}(t'). \tag{2}$$

The ionic displacements are presented here as symmetric coordinates transforming like the ith row of the irreducible representation Γ_α of the cubic group O_h, the index t distinguishing identical representations.

All matrix elements of H_{el} connecting the states with s^2 and sp configurations are expressed through the single-electron matrix elements connecting s or p states. The p (t_{1u}) functions transform according to the Γ_{4u} representation, $[\Gamma_{4u}^2] = \Gamma_{1g} + \Gamma_{3g} + \Gamma_{5g}$; therefore the matrix elements of the operators $V^{(1g)}$, $V_i^{(3g)}$, $V_i^{(5g)}$ may only differ from zero for those functions. Since Γ_{1g}, Γ_{3g}, Γ_{5g} enter $[\Gamma_{4u}^2]$ once, the sets of matrix elements of $V_i^{(\alpha)}(t)$ for different t differ only by a factor (the Wigner–Eckart theorem), so $H_{el}^{(1)}$ may effectively be rewritten as

$$\begin{aligned} H_{el}^{(1)} &= \sum_{\alpha i} V_i^{\alpha} \{c_{1\alpha} Q_i^{(\alpha)}(1) + c_{2\alpha} Q_i^{(\alpha)}(2) + \cdots\} \\ &= V_1 Q_1'(\Gamma_{1g}) + (V_2 Q_2' + V_3 Q_3')(\Gamma_{3g}) + (V_4 Q_4' + V_5 Q_5' + V_6 Q_6')(\Gamma_{5g}). \end{aligned} \tag{3}$$

Here the Q_i' are effective 'interaction modes' (a term coined by Toyozawa and Inoue [13]), composed of all symmetric coordinates of the corresponding type. In the present model the reduced matrix elements of the operators $V_i^{(\alpha)}$ are considered as model parameters, so there is no necessity to restrict the impurity centre to the nearest neighbours of the Tl^+ ion. In what follows we will take into account only the interaction modes; therefore the primes on the Q_i' in (3) will be omitted.

The second-order term $H_{el}^{(2)}$ may be rearranged in a similar manner to $H_{el}^{(1)}$. Retaining, for the sake of brevity, only the interaction modes, we rewrite $H_{el}^{(2)}$ in an effective form:

$$\begin{aligned} H_{el}^{(2)} = {} & V_1^{(1)}Q_1^2 + V_1^{(2)}(Q_2^2+Q_3^2) + V_1^{(3)}(Q_4^2+Q_5^2+Q_6^2) + (V_2^{(1)}Q_2 + V_3^{(1)}Q_3)Q_1 \\ & + (V_4^{(1)}Q_4 + V_5^{(1)}Q_5 + V_6^{(1)}Q_6)Q_1 + V_2^{(2)}2Q_2Q_3 + V_3^{(2)}(Q_2^2-Q_3^2) \\ & + V_4^{(2)}Q_4(-Q_3/2+\sqrt{3}Q_2/2) + V_5^{(2)}Q_5(-Q_3/2-\sqrt{3}Q_2/2) \\ & + V_6^{(2)}Q_6Q_3 + V_2^{(3)}(Q_4^2-Q_5^2) + V_3^{(3)}(2Q_6^2-Q_4^2-Q_5^2)/\sqrt{3} \\ & + V_4^{(3)}Q_5Q_6 + V_6^{(3)}Q_4Q_5 \end{aligned} \tag{4}$$

where the $V_1^{(\alpha)}$ are cubic invariants; the pairs of electronic operators $(V_2^{(\alpha)}, V_3^{(\alpha)})$ and the respective quadratic combinations of Q_i transform according to the Γ_{3g} representation as θ and $\varepsilon[(x^2-y^2), (3z^2-r^2)/\sqrt{3}]$, respectively; the triplets $(V_4^{(\alpha)}, V_5^{(\alpha)}, V_6^{(\alpha)})$ transform as yz, zx, xy according to the Γ_{5g} representation. The electron–lattice Hamiltonian $H_{el} = H_{el}^{(1)} + H_{el}^{(2)}$ may be presented in a unified form:

$$H_{el} = \sum_{i=1,\dots,6} \boldsymbol{V}_i \cdot \boldsymbol{Q}_i \tag{5}$$

if one introduces the '4-vectors'

$$\begin{aligned} \boldsymbol{V}_i &= (V_i, V_i^{(1)}, V_i^{(2)}, V_i^{(3)}) \\ \boldsymbol{Q}_1 &= (Q_1, Q_1^2, Q_2^2+Q_3^2, Q_4^2+Q_5^2+Q_6^2) \\ \boldsymbol{Q}_2 &= (Q_2, Q_1Q_2, 2Q_2Q_3, Q_4^2-Q_5^2) \\ \boldsymbol{Q}_3 &= [Q_3, Q_1Q_3, Q_2^2-Q_3^2, (2Q_6^2-Q_4^2-Q_5^2)/\sqrt{3}] \\ \boldsymbol{Q}_4 &= \left[Q_4, Q_1Q_4, Q_4\left(-\frac{1}{2}Q_3+\frac{\sqrt{3}}{2}Q_2\right)Q_5Q_6\right] \\ \boldsymbol{Q}_5 &= \left[Q_5, Q_1Q_5, Q_5\left(-\frac{1}{2}Q_3-\frac{\sqrt{3}}{2}Q_2\right), Q_4Q_6\right] \\ \boldsymbol{Q}_6 &= (Q_6, Q_1Q_6, Q_3Q_6, Q_4Q_5) \end{aligned} \tag{6}$$

and considers $\boldsymbol{V}_i \cdot \boldsymbol{Q}_i$ as scalar products of those 'vectors'. To consider only the linear Jahn–Teller effect, it is sufficient to restrict H_{el} to the terms $\boldsymbol{V}_1 \cdot \boldsymbol{Q}_1 + \sum V_i Q_i$, $i = 2, \dots, 6$.

An initial set of twelve two-electron functions of the sp configuration for construction of the matrix $(H_{so} + H_{el})$ is usually chosen in the simplest form corresponding to irreducible representations of the O_h group and spin multiplets and diagonalizing $H_0 + H_{ee}$ [13]:

$$\begin{aligned} |^3\Gamma_{1u}\rangle &= \frac{1}{\sqrt{3}}\{|X_-S_x\rangle + |Y_-S_y\rangle + |Z_-S_z\rangle\} \\ |^3\Gamma_{4u}, x\rangle &= \frac{\mathrm{i}}{\sqrt{2}}\{|Y_-S_z\rangle - |Z_-S_y\rangle\} \\ |^3\Gamma_{3u}, \theta\rangle &= \frac{1}{\sqrt{2}}\{|X_-S_x\rangle - |Y_-S_y\rangle\} \\ |^3\Gamma_{3u}, \varepsilon\rangle &= \frac{1}{\sqrt{6}}\{2|Z_-S_z\rangle - |X_-S_x\rangle - |Y_-S_y\rangle\} \\ |^3\Gamma_{5u}, yz\rangle &= \frac{1}{\sqrt{2}}\{|Y_-S_z\rangle + |Z_-S_y\rangle\} \\ |^1\Gamma_{4u}, x\rangle &= |X_+S_0\rangle. \end{aligned} \tag{7}$$

Only one function is given here for the Γ_{4u} and Γ_{5u} representations; other functions are obtained by cyclic permutations of x, y, z. The spin singlet is

$$|S_0\rangle = \frac{1}{\sqrt{2}}\left\{\left|\frac{1}{2},-\frac{1}{2}\right\rangle - \left|-\frac{1}{2},\frac{1}{2}\right\rangle\right\}.$$

The spin-triplet functions are

$$|S_x\rangle = -\frac{1}{\sqrt{2}}\left\{\left|\frac{1}{2},\frac{1}{2}\right\rangle - \left|-\frac{1}{2},-\frac{1}{2}\right\rangle\right\}$$

$$|S_y\rangle = \frac{\mathrm{i}}{\sqrt{2}}\left\{\left|\frac{1}{2},\frac{1}{2}\right\rangle + \left|-\frac{1}{2},-\frac{1}{2}\right\rangle\right\}$$

$$|S_z\rangle = \frac{1}{\sqrt{2}}\left\{\left|\frac{1}{2},-\frac{1}{2}\right\rangle + \left|-\frac{1}{2},\frac{1}{2}\right\rangle\right\}.$$

The orbital two-electron functions are

$$|X_\pm\rangle = \frac{1}{\sqrt{2}}\{|\mathrm{sp}_x\rangle \pm |\mathrm{p}_x\mathrm{s}\rangle\}$$

and so on.

In what follows we will use the following designations of the electron–lattice interaction parameters:

$$\begin{aligned} \boldsymbol{a} &= \langle \mathrm{s}|\boldsymbol{V}_1|\mathrm{s}\rangle + \langle \mathrm{p}_x|\boldsymbol{V}_1|\mathrm{p}_x\rangle \\ \boldsymbol{b} &= \langle \mathrm{p}_x|\boldsymbol{V}_2|\mathrm{p}_x\rangle \\ \boldsymbol{c} &= \langle \mathrm{p}_y|\boldsymbol{V}_4|\mathrm{p}_z\rangle \end{aligned} \tag{8}$$

in the case of triplet functions, and primes will be used for the case of singlet functions. With these designations the matrix of the Hamiltonian (1) based on the state functions (7) is as follows:

$$\begin{pmatrix} \langle {}^3\Gamma_{1u}| \\ \langle {}^3\Gamma_{4u}| \\ \langle {}^3\Gamma_{3u}| \\ \langle {}^3\Gamma_{5u}| \\ \langle {}^1\Gamma_{4u}| \end{pmatrix} \begin{pmatrix} \mathcal{A}-\zeta/2 & 0 & (H_{13}) & (H_{14}) & 0 \\ 0 & \mathcal{A}+(H_{22}) & (H_{23}) & (H_{24}) & \lambda\zeta/\sqrt{2} \\ (H_{31}) & (H_{32}) & \mathcal{B}+(H_{33}) & (H_{34}) & 0 \\ (H_{41}) & (H_{42}) & (H_{43}) & \mathcal{B}+(H_{44}) & 0 \\ 0 & \lambda\zeta/\sqrt{2} & 0 & 0 & \mathcal{C}+(H_{55}) \end{pmatrix} \tag{9}$$

where

$$\begin{aligned} \mathcal{A} &= E_\mathrm{A} + \boldsymbol{a}\cdot\boldsymbol{Q}_1 \\ \mathcal{B} &= E_\mathrm{B} + \boldsymbol{a}\cdot\boldsymbol{Q}_1 \\ \mathcal{C} &= E_\mathrm{C} + \boldsymbol{a}'\cdot\boldsymbol{Q}_1. \end{aligned}$$

Here ζ is a spin–orbit coupling constant; the factor λ takes into account the difference between radial functions in singlet and triplet spin states. The energies $E_{\mathrm{A,B,C}}$ are shown in figure 2 and may be expressed through Coulomb (F) and exchange (G) integrals. The submatrices

$(H_{ij}) = (H_{ji})^+$ have the following forms:

$$
\begin{aligned}
(H_{13}) &= \sqrt{\frac{2}{3}}(\boldsymbol{b}\cdot\boldsymbol{Q}_2, \boldsymbol{b}\cdot\boldsymbol{Q}_3)\\
(H_{14}) &= \sqrt{\frac{2}{3}}(\boldsymbol{c}\cdot\boldsymbol{Q}_4, \boldsymbol{c}\cdot\boldsymbol{Q}_5 \boldsymbol{c}\cdot\boldsymbol{Q}_6)\\
(H_{22}) &= \begin{pmatrix} \langle {}^3\Gamma_{4u}, x| \\ \langle {}^3\Gamma_{4u}, y| \\ \langle {}^3\Gamma_{4u}, z| \end{pmatrix} \begin{vmatrix} -\frac{1}{2}\boldsymbol{b}\cdot(\boldsymbol{Q}_2 - \frac{1}{\sqrt{3}}\boldsymbol{Q}_3) & -\frac{1}{2}\boldsymbol{c}\cdot\boldsymbol{Q}_6 & -\frac{1}{2}\boldsymbol{c}\cdot\boldsymbol{Q}_5 \\ -\frac{1}{2}\boldsymbol{c}\cdot\boldsymbol{Q}_6 & \frac{1}{2}\boldsymbol{b}\cdot(\boldsymbol{Q}_2 + \frac{1}{\sqrt{3}}\boldsymbol{Q}_3) & -\frac{1}{2}\boldsymbol{c}\cdot\boldsymbol{Q}_4 \\ -\frac{1}{2}\boldsymbol{c}\cdot\boldsymbol{Q}_5 & -\frac{1}{2}\boldsymbol{c}\cdot\boldsymbol{Q}_4 & -\frac{1}{\sqrt{3}}\boldsymbol{b}\cdot\boldsymbol{Q}_3 \end{vmatrix}.
\end{aligned}
\tag{10}
$$

The matrix (H_{44}) is obtained from (H_{22}) by changing the sign before $\boldsymbol{c}$, and (H_{55}) is obtained from (H_{22}) by making the changes $\boldsymbol{b}/2 \to -\boldsymbol{b}'$, $\boldsymbol{c}/2 \to -\boldsymbol{c}'$. Further,

$$
\begin{aligned}
(H_{33}) &= \begin{pmatrix} \langle {}^3\Gamma_{3u}, \theta| \\ \langle {}^3\Gamma_{3u}, \varepsilon| \end{pmatrix} \begin{vmatrix} -\frac{1}{\sqrt{3}}\boldsymbol{b}\cdot\boldsymbol{Q}_3 & -\frac{1}{\sqrt{3}}\boldsymbol{b}\cdot\boldsymbol{Q}_2 \\ -\frac{1}{\sqrt{3}}\boldsymbol{b}\cdot\boldsymbol{Q}_2 & \frac{1}{\sqrt{3}}\boldsymbol{b}\cdot\boldsymbol{Q}_3 \end{vmatrix}\\
(H_{32}) &= \begin{vmatrix} \frac{\mathrm{i}}{2}\boldsymbol{c}\cdot\boldsymbol{Q}_4 & \frac{\mathrm{i}}{2}\boldsymbol{c}\cdot\boldsymbol{Q}_5 & -\mathrm{i}\boldsymbol{c}\cdot\boldsymbol{Q}_6 \\ \mathrm{i}\frac{\sqrt{3}}{2}\boldsymbol{c}\cdot\boldsymbol{Q}_4 & -\mathrm{i}\frac{\sqrt{3}}{2}\boldsymbol{c}\cdot\boldsymbol{Q}_5 & 0 \end{vmatrix}\\
(H_{24}) &= \begin{vmatrix} \frac{\mathrm{i}}{2}\boldsymbol{b}\cdot(\boldsymbol{Q}_2 + \sqrt{3}\boldsymbol{Q}_3) & -\frac{\mathrm{i}}{2}\boldsymbol{c}\cdot\boldsymbol{Q}_6 & \frac{\mathrm{i}}{2}\boldsymbol{c}\cdot\boldsymbol{Q}_5 \\ \frac{\mathrm{i}}{2}\boldsymbol{c}\cdot\boldsymbol{Q}_6 & \frac{\mathrm{i}}{2}\boldsymbol{b}\cdot(\boldsymbol{Q}_2 - \sqrt{3}\boldsymbol{Q}_3) & -\frac{\mathrm{i}}{2}\boldsymbol{c}\cdot\boldsymbol{Q}_4 \\ -\frac{\mathrm{i}}{2}\boldsymbol{c}\cdot\boldsymbol{Q}_5 & \frac{\mathrm{i}}{2}\boldsymbol{c}\cdot\boldsymbol{Q}_4 & -\mathrm{i}\boldsymbol{b}\cdot\boldsymbol{Q}_2 \end{vmatrix}\\
(H_{34}) &= \begin{vmatrix} -\frac{1}{2}\boldsymbol{c}\cdot\boldsymbol{Q}_4 & \frac{1}{2}\boldsymbol{c}\cdot\boldsymbol{Q}_5 & 0 \\ \frac{1}{2\sqrt{3}}\boldsymbol{c}\cdot\boldsymbol{Q}_4 & \frac{1}{2\sqrt{3}}\boldsymbol{c}\cdot\boldsymbol{Q}_5 & -\frac{1}{\sqrt{3}}\boldsymbol{c}\cdot\boldsymbol{Q}_6 \end{vmatrix}.
\end{aligned}
\tag{11}
$$

The twelve-dimensional matrix (9) with submatrices (10) and (11) coincides with that in the literature [3] except for some corrections and an extended redefinition of the parameters $\boldsymbol{a}$, $\boldsymbol{b}$, $\boldsymbol{c}$ and coordinates $\boldsymbol{Q}$, which allows us to take into account the quadratic Jahn–Teller effect.

For some applications, another set of functions that diagonalize the Hamiltonian $H_0 + H_{ee} + H_{so}$ appears to be more convenient:

$$
\begin{aligned}
|{}^3\Gamma^*_{4u}, i\rangle &= \mu|{}^3\Gamma_{4u}, i\rangle - \nu|{}^1\Gamma_{4u}, i\rangle\\
|{}^1\Gamma^*_{4u}, i\rangle &= \mu|{}^1\Gamma_{4u}, i\rangle + \nu|{}^3\Gamma_{4u}, i\rangle
\end{aligned}
\tag{12}
$$

where

$$
\begin{aligned}
&\mu^2/\nu^2 \equiv R = (2\Delta + E_{CA})/(2\Delta - E_{CA})\\
&2\Delta = \sqrt{E_{CA}^2 + 2\lambda^2\zeta^2} \qquad \mu^2 + \nu^2 = 1.
\end{aligned}
$$

The corresponding eigenvalues for the states $|{}^3\Gamma^*_{4u}\rangle$ and $|{}^1\Gamma^*_{4u}\rangle$ are

$$
E^*_{C,A} = \frac{1}{2}(E_A + E_C) \pm \Delta.
$$

The displacements of ions from their equilibrium positions during lattice vibrations result in random changes (fluctuations) of the electronic spectrum of the impurity centre. The energy spectrum obtained by diagonalization of the matrix (9) for a given set of coordinates $\widetilde{Q}(Q_1 - Q_6)$ defines the momentary absorption spectra with δ-shaped lines for an absorption centre with these Qs. There are twelve excited 'stationary' states (enumerated by index

$j = 1, \ldots, 12$ in order of energy increase) which are the linear combinations of the initial set of functions (7):

$$|\psi_j\rangle = \sum_{\alpha i} C_{\alpha i,j}(\widetilde{Q})|\alpha, i\rangle. \tag{13}$$

Since the electric dipole transitions from the ground state $|^1\Gamma_{1g}\rangle$ are allowed only to singlet excited states $|^1\Gamma_{4u}, x, y, z\rangle$, the intensity for transition to a $|\psi_j\rangle$ state is proportional to the squared absolute values of the coefficients $C_{\alpha i,j}$ with $\alpha = {}^1\Gamma_{4u}$. The observed form of the absorption spectra for non-polarized radiation is a result of averaging over all fluctuations Q:

$$F(\omega) = \sum_j \frac{1}{3}\int \mathrm{d}w(\widetilde{Q}) \sum_{i=x,y,z} |C(^1\Gamma_{4u}, i, j)|^2 \delta[\hbar\omega - E_j(\widetilde{Q})] \tag{14}$$

where $\mathrm{d}w(\widetilde{Q})$ is a fluctuation probability. In the thermodynamic equilibrium state the probability is distributed according to the Gaussian law:

$$\mathrm{d}w(\widetilde{Q}) = \prod_\alpha \frac{1}{\sqrt{2\pi\langle Q_\alpha^2\rangle}} \exp\left(-\frac{Q_\alpha^2}{2\langle Q_\alpha^2\rangle}\right) \mathrm{d}Q_\alpha \tag{15}$$

where $\langle Q_\alpha^2\rangle$ is, in appropriate units, a mean value of elastic energy connected with the displacement Q_α.

In the classic (high-temperature) limit $\langle Q_\alpha^2\rangle = kT/2$, but at low temperatures the contribution of zero vibrations to displacements becomes significant. It may be accounted for approximately by changing T to an effective temperature which is the mean energy of an oscillator with an averaged frequency: $kT^* = (\hbar\omega_{eff}/2)\coth(\hbar\omega_{eff}/2kT)$ [3]. However, introduction of a single effective frequency for interaction modes seems to be a rather crude approximation which can substantially distort the temperature dependence of the calculated parameters of the spectra. We think that it is more reasonable to couple a proper frequency with each of three modes Γ_{1g}, Γ_{3g} and Γ_{5g}:

$$2\langle Q_\alpha^2\rangle = \frac{1}{2}\hbar\omega_\alpha \coth\left(\frac{\hbar\omega_\alpha}{2kT}\right). \tag{16}$$

Therefore in this model, the absorption spectrum form (14) is defined by the following parameters of the energy matrix (9):

$$E_A, E_B, E_C, \lambda\zeta, \boldsymbol{a}(a, a_1, a_2, a_3), \boldsymbol{b}, \boldsymbol{c}, \boldsymbol{a}', \boldsymbol{b}', \boldsymbol{c}'(a_1 \equiv a^{(1)}, \text{etc})$$

and three effective frequencies $\omega_1(\Gamma_{1g})$, $\omega_2(\Gamma_{3g})$, $\omega_3(\Gamma_{5g})$ associated with each active mode of impurity centre vibrations.

As mentioned above, the mean squared fluctuation of the ion positions in a crystal at high temperatures is of the order of kT, so the mean splitting $c\sqrt{\langle Q^2\rangle}$ of impurity levels due to H_{el} approximately equals 0.2 eV even for comparatively high values of electron–lattice interaction ($c^2 \approx 2$ eV), which is substantially less than the energy intervals E^*_{BA} and E^*_{CA}. Therefore the diagonalization of the energy matrix can be carried out by use of the perturbation theory as was done in the original work of Toyozawa and Inoue [13]. The three-dimensional matrix defining energies of A-band states in the second order is as follows:

$$(H_A) = \langle {}^3\Gamma^*_{4u}|H|{}^3\Gamma^*_{4u}\rangle + \sum_\alpha{}' \frac{\langle {}^3\Gamma^*_{4u}|H_{el}|\Gamma_\alpha\rangle\langle\Gamma_\alpha|H_{el}|{}^3\Gamma^*_{4u}\rangle}{E^*_A - E(\Gamma_\alpha)} \tag{17}$$

where the functions (12) are used for writing down the blocks of the (H_{el}) matrix.

To lower the number of fitting parameters, let us consider only the linear Jahn–Teller effect. Then the matrix (H_A) is as follows:

$$
\begin{aligned}
&(H_A) = E_A^* + AQ_1 + A_1Q_1^2 + A_2(Q_2^2+Q_3^2) + A_3(Q_4^2+Q_5^2+Q_6^2) + (H^A)\\
&H_{11}^A = B\left(Q_2 - \frac{1}{\sqrt{3}}Q_3\right) + B_2\left[2Q_2Q_3 - \frac{1}{\sqrt{3}}(Q_2^2-Q_3^2)\right] + \frac{2}{3}B_3(2Q_4^2-Q_5^2-Q_6^2)\\
&H_{12}^A = CQ_6 + C_2Q_6Q_3 + C_3Q_4Q_5\\
&H_{13}^A = CQ_5 + C_2Q_5\left(-\frac{1}{2}Q_3 - \frac{\sqrt{3}}{2}Q_2\right) + C_3Q_4Q_6\\
&H_{22}^A = B\left(-Q_2 - \frac{1}{\sqrt{3}}Q_3\right) + B_2\left[-2Q_2Q_3 - \frac{1}{\sqrt{3}}(Q_2^2-Q_3^2)\right] + \frac{2}{3}B_3(2Q_5^2-Q_4^2-Q_6^2)\\
&H_{23}^A = CQ_4 + C_2Q_4\left(-\frac{1}{2}Q_3 + \frac{\sqrt{3}}{2}Q_2\right) + C_3Q_5Q_6\\
&H_{33}^A = \frac{2}{\sqrt{3}}BQ_3 + \frac{2}{\sqrt{3}}B_2(Q_2^2-Q_3^2) + \frac{2}{3}B_3(2Q_6^2-Q_5^2-Q_4^2)
\end{aligned}
\tag{18}
$$

where

$$
\begin{aligned}
A &= a'\nu^2 + a\mu^2\\
A_1 &= a_1'\nu^2 + a_1\mu^2\\
A_2 &= a_2'\nu^2 + a_2\mu^2 + \frac{1}{2}\mu^2\frac{b^2}{E_A^*-E_B} + \frac{2}{3}\mu^2\nu^2\frac{(b'+\frac{1}{2}b)^2}{E_A^*-E_C^*}\\
A_3 &= a_3'\nu^2 + a_3\mu^2 + \frac{1}{2}\mu^2\frac{c^2}{E_A^*-E_B} + \frac{2}{3}\mu^2\nu^2\frac{(c'+\frac{1}{2}c)^2}{E_A^*-E_C^*}\\
B &= b'\nu^2 - \frac{1}{2}b\mu^2\\
B_2 &= \frac{\sqrt{3}}{4}\mu^2\frac{b^2}{E_A^*-E_B} - \frac{1}{\sqrt{3}}\mu^2\nu^2\frac{(b'+\frac{1}{2}b)^2}{E_A^*-E_C^*}\\
B_3 &= \frac{3}{8}\mu^2\frac{c^2}{E_A^*-E_B} - \frac{1}{2}\mu^2\nu^2\frac{(c'+\frac{1}{2}c)^2}{E_A^*-E_C^*}\\
C &= c'\nu^2 - \frac{1}{2}c\mu^2\\
C_2 &= \frac{\sqrt{3}}{2}\mu^2\frac{bc}{E_A^*-E_B} - \frac{2}{\sqrt{3}}\mu^2\nu^2\frac{(b'+\frac{1}{2}b)(c'+\frac{1}{2}c)}{E_A^*-E_C^*}\\
C_3 &= -\frac{3}{4}\mu^2\frac{c^2}{E_A^*-E_B} + \mu^2\nu^2\frac{(c'+\frac{1}{2}c)^2}{E_A^*-E_C^*}.
\end{aligned}
\tag{19}
$$

The form function of the absorption A band up to a normalization factor equals

$$
F_A(\omega) = \sum_{j=1,2,3}\int \mathrm{d}w(\widetilde{Q})\,\delta[\hbar\omega - E_{j0}(\widetilde{Q})] \tag{20}
$$

where $E_{j0}(\widetilde{Q}) = E_j(\widetilde{Q}) - E_0(\widetilde{Q})$, $E_j(\widetilde{Q})$ are the eigenvalues of the matrix (18), $E_0(\widetilde{Q}) = \sum_i Q_i^2$ is the energy of the ground state. Of course, the total absorption spectrum may be obtained by diagonalizing the 12×12 matrix (9) and with a form function (14) (see, for

instance, [12]). When the perturbation procedure is applicable, the spectrum calculated in such a manner consists of three well separated bands with form functions (up to a normalization factor) F_A (F_C) very close to that given by equation (20). In this work, we deal mainly with the absorption A band and therefore use the simplified procedure of band-shape calculation given above. The shape of the C band can be calculated in a similar manner.

The quadratic Jahn–Teller effect can be taken into account by minimal changes of the matrix (18). For instance, the term $b_2'\nu^2 - (1/2)b_2\mu^2$ is added to the coefficient B_2 (B_3, C_2, C_3 undergo analogous changes), leaving its structure unchanged. One may conclude that taking into account the quadratic Jahn–Teller effect does not change the qualitative results from the conventional linear model (cf. [2, 3]).

4. Numerical calculations of absorption spectra and discussion

We have calculated the A-band shape $F_A(\omega)$ (20) for the crystals studied with the Monte Carlo method. The matrix (18) was diagonalized for each random set $\widetilde{Q}$ in a six-dimensional space chosen in accordance with the distribution (15), the total number of sets being 400 000. The value $F_A(\omega)$ is proportional to the number of energy values $E_{j0}(\widetilde{Q})$ falling into the small range $(\omega, \omega + d\omega)$.

For calculation of the shape of the A band for $KZnF_3$:Tl^+, the following set of parameters was used:

$$\begin{array}{lll} E_A^* = 6.03\ \text{eV} & E_B = 7.2\ \text{eV} & E_C^* = 8.14\ \text{eV} \\ R = 7 & & \\ a^2 = a'^2 = 0.023\ \text{eV} & b^2 = 0.49\ \text{eV} & b'^2 = 0.25\ \text{eV} \\ c^2 = 1.69\ \text{eV} & c'^2 = 1\ \text{eV} & \\ a_i = a_i' = 0.8 & i = 1, 2, 3 & \\ \omega(\Gamma_1, \Gamma_3) = 300\ \text{cm}^{-1} & \omega(\Gamma_5) = 100\ \text{cm}^{-1}. & \end{array} \tag{21}$$

The calculation results are compared with experimental ones in figure 5.

The experimental data for $KMgF_3$:Tl^+ were fitted with the following set of theoretical parameters:

$$\begin{array}{lll} E_A^* = 6.15\ \text{eV} & E_B = 7.38\ \text{eV} & E_C^* = 8.27\ \text{eV} \\ R = 7 & & \\ a^2 = a'^2 = 0.023\ \text{eV} & b^2 = 0.81\ \text{eV} & b'^2 = 0.49\ \text{eV} \\ c^2 = 1.96\ \text{eV} & c'^2 = 1.21\ \text{eV} & \\ a_i = a_i' = 0.9 & i = 1, 2, 3 & \\ \omega(\Gamma_1, \Gamma_3) = 300\ \text{cm}^{-1} & \omega(\Gamma_5) = 100\ \text{cm}^{-1}. & \end{array} \tag{22}$$

The calculation results are compared with experimental data and calculations of [12], where somewhat different parameters were used and only the temperature of 9 K was considered (figure 6). There is satisfactory qualitative and, to some extent, quantitative agreement between the experimental and calculated curves. Figure 6 shows that parameters (22) lead to a better agreement with experimental data for temperatures $T = 150$ and 300 K than the parameters of [12]. The strong broadening of the band and shift to higher energies with increase of temperature are evidently due to a too high value of the curvature of the excited-state parabola $k_e = 2.1$ being used in [12].

We have also calculated the C-band shape for $KMgF_3$:Tl^+ with the parameters given in (22). The agreement with the experimental results of Scacco *et al* [10] is similar to that given

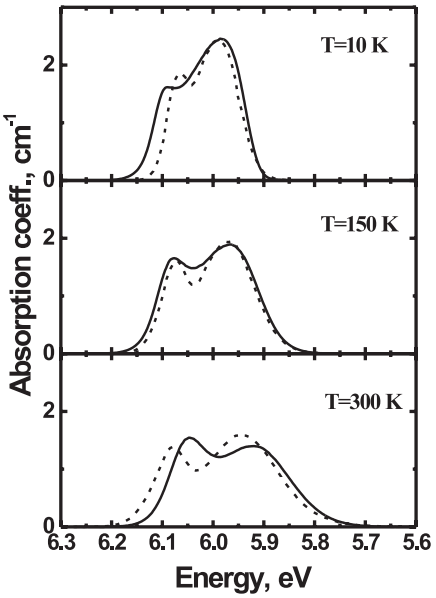

Figure 5. Absorption spectra of the $KZnF_3:Tl^+$ crystal (solid curves) and their simulations with the parameters of the present work (dashed curves).

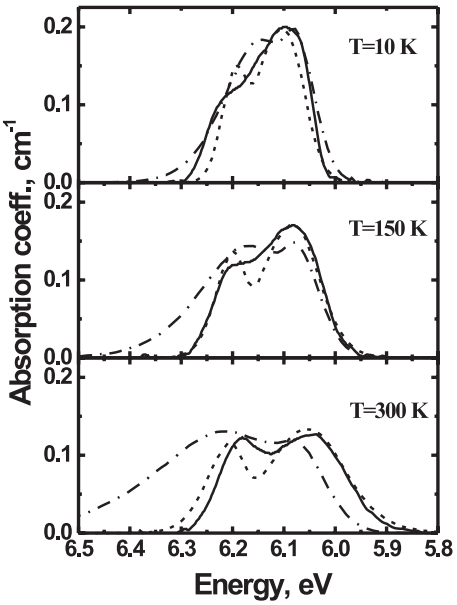

Figure 6. Absorption spectra of the $KMgF_3:Tl^+$ crystal (solid curves) and their simulations with the parameters of the present work (dashed curves) and those of [12] (dot-and-dash curves).

above for the A band. Again, the calculations with the parameters of [12] result in significant overestimation of the bandwidth for high temperatures.

The parameters E_A^*, E_B, E_C^* for $KMgF_3:Tl^+$ were chosen in accordance with the absorption band positions [10]. The parameter $\mu^2/\nu^2 \equiv R$ is approximately equal to the ratio of integral intensities of the C and A bands and its experimental value is $R = 4.8$; we take a somewhat larger value $R = 7$ which corresponds better to the chosen energy values. Only one energy parameter $E_A^* = 6.03$ eV was fixed experimentally for $KZnF_3:Tl^+$. The values of E_B and E_C^* in (21) are obtained by the appropriate shift of the energy levels for $KMgF_3:Tl^+$.

The values in (21) and (22) show that the coupling with Γ_{5g} vibration modes prevails in the electron–lattice interaction of the crystals studied. This could have been anticipated because of the observed distinct structure of the absorption bands, since Toyozawa and Inoue showed [13] that only the coupling to trigonal (Γ_{5g}) modes gives rise to that structure. The noticeable temperature dependence of the band structure, which begins at temperatures of $\sim$70 K, allows us to conclude that the effective frequency $\omega(\Gamma_{5g})$ is not high, since according to equation (16) the effective temperature T_α^* does not depend on T in the temperature range $(0, \omega_\alpha/2)$. Therefore $\omega(\Gamma_{5g}) \leqslant 140$ K (100 cm^{-1}) and the chosen value $\omega(\Gamma_{5g}) = 100$ cm^{-1} allows us to obtain a satisfactory description of both the band structure and the bandwidth. The low-frequency quasilocal vibration may be due to the introduction of the heavy Tl^+ ion in place of the K^+ ion.

The experimental data do not allow us to fix electron–lattice interaction parameters very precisely. It is possible to change the value of one parameter (say c^2) by about a factor of two and to change other parameters accordingly without causing serious deterioration of the calculation results. Therefore the values of the parameters a, b, c etc given in (21), (22) should be considered as very approximate ones.

5. Summary

Absorption spectra of $KZnF_3:Tl^+$ and $KMgF_3:Tl^+$ crystals identified as absorption A bands of Tl^+ impurity centres were observed in the near-UV region. The band shapes for the two crystals are similar: they have temperature-dependent doublet structures and bandwidths. The absorption band in $KZnF_3:Tl^+$ is observed at somewhat lower energies than that in $KMgF_3:Tl^+$.

All features of the absorption spectra in the crystals studied are satisfactorily explained within the frameworks of the conventional theory on the basis of the Frank–Condon principle and the semiclassical picture of crystal lattice vibrations. Minimal modifications allow us to consider in a unified way the linear electron–lattice interactions and those quadratic in atomic displacements and to take into account the differences between the effective frequencies of the interaction modes. The smallest frequency is defined approximately by the temperature at which the band shape becomes temperature independent. The electron–lattice interaction parameters are estimated from experiment with accuracy up to a factor of about 2.

Acknowledgment

This work was supported by the Russian Foundation for Basic Research, grant No 98-02-18037.

References

[1] Fowler W B 1968 *Physics of Color Centers* (New York: Academic)
[2] Ranfagni A, Mugnai P, Bacci M, Viliani G and Fontana M P 1983 *Adv. Phys.* **32** 823
[3] Jacobs P W M 1991 *J. Phys. Chem. Solids* **52** 35
[4] Horsch G and Paus H J 1986 *Opt. Commun.* **60** 69
[5] Demchuk M U, Kuleshov N V, Mikhailov V P, Haidukov N M, Shkadarevich A P and Sherbinski V G 1990 *Zh. Prikl. Spectrosk.* **53** 375
[6] Furetta C, Bacci C, Rispoli B, Sanipoli C and Scacco A 1990 *Radiat. Protect. Dosim.* **33** 107
[7] Mityagin M V, Nikitin S I, Silkin N I, Shkadarevich A P and Yagudin Sh I 1990 *Izv. Akad. Nauk SSSR, Ser. Phys.* **54** 1512
[8] German K R, Durr U and Kunzel W 1986 *Opt. Lett.* **11** 12
[9] Johnson L F, Guggenheim H J, Bahnek D and Johnson A M 1983 *Opt. Lett.* **8** 371
[10] Scacco A, Fioravanti S, Missori M, Grassano U M, Luci A, Palummo M, Giovenale E and Zema N 1993 *Phys. Chem. Solids* **54** 1035
[11] Scacco A, Fioravanti F, Grassano U M, Zema N, Nikl M, Mihokova E and Hamplova V 1994 *Phys. Chem. Solids* **55** 1
[12] Tsuboi T and Scacco A 1995 *J. Phys.: Condens. Matter* **7** 9321
[13] Toyozawa Y and Inoue M 1966 *J. Phys. Soc. Japan* **21** 1663